Journal of Materials Chemistry C

Accepted Manuscript

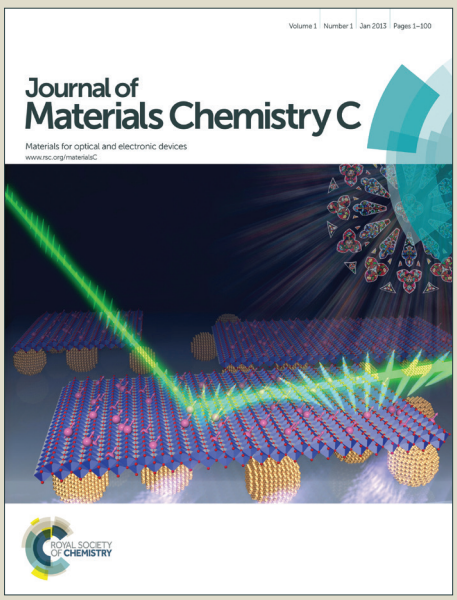

ROYAL SOCIETY OF CHEMISTRY

www.rsc.org/materialsC

Ambipolar Field-Effect Transistors Using Conjugated Polymers with the Structures of Bilayer, Binary Blends, and Paralleled Nanofibers†

Chien Lu,[1] Jin Wang,[2] Hsuan-Chun Chang,[1] Yu-Cheng Chiu,[1] Hsueh-Yung Chen,[1] Hung-Chin Wu,[1] Tomoya Higashihara,[2,*] and Wen-Chang Chen[1,*]

[1]Department of Chemical Engineering, National Taiwan University, Taipei, 10617, Taiwan

[2]Department of Polymer Science and Engineering/Organic Device Engineering, Yamagata University, 4-3-16 Jonan Yonezawa, Yamagata-ken 992-8510 Japan

* To whom all correspondence should be addressed.

E-mail:chenwc@ntu.edu.tw (W.-C. Chen), thigashihara@yz.yamagata-u.ac.jp (T. Higashihara)

Abstract

In this paper, we explore the ambipolar organic field-effect transistor (FET) characteristics using the bilayer, binary blends, and paralleled nanofibers of poly(3-hexylthiophene) (P3HT; p-type) and poly{[N,N'-bis(2-decyltetradecyl)-naphthalene-1,4,5,8-bis(dicarboximide)-2,6-diyl] -*alt*-(thiophene-2,5-diyl)} (P(NDI-T); n-type). The ambipolar transistors with paralleled single P3HT and P(NDI-T) electrospun nanofibers showed high and well-balanced mobilities of 8.25×10^{-2}cm^2/V s for holes and 7.51×10^{-2}cm^2/V s for electrons with $I_{on}/I_{off}\sim10^4$. This ambipolar nanofiber FET was also applied into complementary inverter with the gain up to 20.5.

Ambipolar field-effect transistor (FET) devices have attracted intensive research efforts in the applications on integrated circuits, radio frequency identification tags, sensors, and memories using cost-effective graphic art printing processes.[1] Recently, organic ambipolar electronics have been fabricated with single materials,[2,3] bilayer structure,[4-8] or binary blends[9-13] as semiconducting active layers. For the heterojunction configuration such as bilayers and binary blends, the charge redistribution occurs at the interface of electron- and hole-transporting layers, leading to charge accumulation or depletion effects.[14] For charge accumulation, mobile electrons in n-type layer and holes in p-type layer have been observed, and would transfer into normally-on characteristics of organic transistors. Nichel and his coworkers proved that the ambipolar characteristics of bilayer FET crucially depend on the film thickness of p-channel (pentacene) and n-channel (C_{60}) semiconductors, controlling the charge density near the p/n interface.[15] The ambipolar FET using binary blends system with poly(3-hexylthiophene) (P3HT) and poly{[N,N'-bis(2-octyldodecyl)-naphthalene-1,4,5,8-bis(dicarbox-imide)-2,6-diyl]-alt-5,5'-(2,2'-bithiophene)} (P(NDI2OD-T2)) were also introduced for balanced electron and hole mobilities of

0.004 and 0.002 cm^2/V s, respectively.[12] Nevertheless, how to choose suitable materials and achieve well-balanced mobilities are still challenging issues for ambipolar organic FET.

Although above mentioned ambipolar FET exhibit balanced charge carrier mobilities, some obstacles such as low on/off ratio and high leakage currents are still existed in commercially integrated circuits. Highly-aligned electrospun nanofibers could be a facile route to isolate the hole and electron channels individually without contacts. In addition, the geometrical confinement of conjugated polymer-based electrospun nanofibers could lead to the enhancement in electronic and optoelectronic properties.[16-18] In our previous work, the two-fluid coaxial electrospinning technique using P3HT as core and poly(methyl methacrylate) (PMMA) as shell was employed to fabricate nanofibers of P3HT with the hole mobility of P3HT to 0.192 cm^2/V s.[19] Additionally, the electron-transporting nanofibers based FET using the blending mixture of P(NDI2-T2) and PEO was also reported to have the mobility of 0.08 cm^2/V s.[20]

Herein, we explored the fabrication and characteristics of solution processable ambipolar FETs with three p/n device architectures of bilayer, binary blends, and paralleled nanofibers, as shown in Fig. 1. P3HT and poly{[N,N'-bis(2-decyltetradecyl)-naphthalene-1,4,5,8-bis(dicarboximide) -2,6-diyl]-*alt*-(thiophene-2,5-diyl)} (P(NDI-T))[21] served as p-type and n-type polymer semiconductors, respectively. Scanning electron microscopy (SEM) was used to determine the integrated structure of the p/n bilayer (cross section) and binary blends at the contact interface of P3HT and P(NDI-T). The surface image of binary blends thin film showed a very fine interpenetrating network of P3HT and P(NDI-T) with two phases, indicating phase segregation between the n-type and p-type materials.[12,22] Nevertheless, the large contact area between two polymers suggests that electrons and holes are expected to recombine at the interface, which would affect the charge transporting behavior of ambipolar transistors. The cross-section image of the bilayer configuration of P(NDI-T) above P3HT with the thickness of 58 nm and 25 nm, respectively. The large thickness difference, which would strongly affect the ambipolar characteristics, could be attributed to the high viscosity of P(NDI-T) solution on the 1,2-propylene glycol buffer layer.[23]

However, it is still very possible that charge capture occurs at the p/n interface.

In order to reduce the chance of charge recombination and current leakage, we propose a new ambipolar transistor device with producing polymer nanofibers through the two-fluid coaxial electrospun technique consisting of conjugated polymer core and PMMA shell followed by extraction of PMMA.[19] The optical microscope (OM) image was taken to confirm the existence and locate the distribution of prepared P3HT and P(NDI-T) nanofibers (Fig. S1(b) in ESI†). The individual aligned fibers are vertically across the gold electrode. The diameter of nanofibers at 0.1 mL/h core feed rate were, estimated by the SEM images (Fig. 1), around 157 nm and 90 nm for P3HT and P(NDI-T), respectively. The internal structures of the prepared P(NDI-T) nanofibers were probed by WAXS. As shown in Fig. S1(a), three diffraction peaks indexed as (100) ,(200), (010) are observable for all nanofibers studied with lamellar d-spacing of 20.3 Å and π-π stacking d-spacing of 3.6 Å, indicating the crystalline lamellar structure in the nanofibers. Note that the P3HT nanofibers also possesses crystalline packing structure, as explored in our previous work.[19] The transistor of single P(NDI-T) nanofiber exhibited electron mobility (μ_e) = 8.15×10^{-2} cm^2/V s, ON/OFF current ratio (I_{on}/I_{off}) = 3.4×10^4, threshold voltage (V_{th}) = 12.27 V at drain voltage (V_d) = 30 V. Compared with the reported value of the transistor with thin film device configuration, the mobility and crystallinity were elevated obviously by this core-shell electrospinning method. Moreover, we can get extremely isolated channels for holes and electrons through collecting the highly-aligned nanofibers. As a result, the possibility of charge recombination could be totally neglected.

The three transistor architectures were fabricated in top contact/bottom gate configuration. The transfer characteristics and the output characteristics of three structures of FET devices are shown in Fig. 2 and Fig. S2 in ESI†, respectively. The transfer characteristics of the bilayer and the binary blends transistor devices obviously showed unideal ambipolar behaviors and exhibited similar hole and electron mobility. The devices exhibit the field effect mobilities of (at V_d = -30 V) 1.09×10^{-4} cm^2/V s of holes and 5.11×10^{-5} cm^2/V s of electrons for the bilayer device, and 5.28×10^{-5} cm^2/V s of holes and 1.77×10^{-5} cm^2/V s of electrons for the device of binary blends. Note that the mobilities and

other electrical performances were calculated in a range of 10 V and averaged from at least five devices, which would not be affected by the sudden drop or rise in the curves. Two phenomena could be observed from the figures on the bilayer and binary blends systems. First, the asymmetric curve indicated the unbalance charge mobilities, which are lower than the reported value of P3HT and P(NDI-T) FET. That might give rise to intermixing of the channels of two polymers, which hinder charge transporting in both channels. Second, because the charge recombination elevated the off current and form serious current leakage, the transfer curves did not show clear cutoff point and the I_{on}/I_{off} ratio were both lower than 10^2 which is unsuitable for transistor application.[24] These unexpected values of the I_{on}/I_{off} ratio possibly result from intermixing network in heterojunction of binary blends and contact interface in bilayer configuration, respectively, in which the P(NDI-T) and P3HT contact directly. However, the energy levels P(NDI-T) and P3HT might lead to the band bending and charge-accumulation at interface, shown in Fig. 2(d). When both holes and electron were transporting in the opposite direction under the same gate bias, the hole and electron capture would easily occur due to the low energy gap difference between HOMO of P3HT and LUMO of P(NDI-T) after band bending.[14] Therefore, the quenching of the generated charges may significantly occur in the two systems to show approximate ohmic behavior in the FET characteristics.

The paralleled p/n electrospun nanofiber-based FET with symmetric transfer characteristics exhibited well-balanced hole-transport (μ_h= 8.25×10^{-2}cm^2/V s, I_{on}/I_{off}= 4.8×10^4, V_t= -8.8V at V_d = -30 V), and electron-transport (μ_e = 7.51×10^{-2}cm^2/V s, I_{on}/I_{off} = 1.5×10^4, V_t= 18.1V at V_d = 30 V) characteristics, showing the enhancement of charge transporting properties from core-shell electrospinning method (Fig. 2(c)). The rough current curves around the cutoff point are attributed to the detection limit of the measuring instrument since the off current of the nanofibers based FETs is lower than 10^{-12} A. Note that the I_{on}/I_{off} ratio for hole and electron are both much higher than that of a fore mentioned transistors of bilayer and binary blends, showing that the extremely isolation of p/n nanofibers could prevent from the capture of holes and electrons and ohmic behavior in the FET characteristics. The band bending did not occur because holes transported only in P3HT nanofiber

and electrons transported only in P(NDI-T) nanofiber, shown in Fig. 2(e). The typical ambipolar behavior has been observed for not only well-balanced hole and electron mobilities but also extremely high I_{on}/I_{off} ratios through employing electrospun nanofiber transistors. As a result, the characterization of the thin film and electrospun nanofibers could provide deep insights on the configurations of these ambipolar transistors, allowing more varied structure choices for ambipolar organic FET in the future.

To demonstrate the feasibility of using electrospun nanofiber-based ambipolar FET in complementary circuits, an inverter with two charge transporting channels was built.[26] The two highly-aligned p- and n-type nanofibers were collected and thermally evaporated with gold electrode on to the nanofibers (Fig. 3). The SEM image of Fig. S3 (ESI†) showed that the two highly-aligned nanofibers were collected at the two sides of electrodes and both the two terminal of inverters contained a P3HT nanofiber and a P(NDI-T) nanofiber. For operating the devices, the input voltage (V_{in}) was applied to the common gate for both transistors in the circuit. When positive V_{DD} and V_{in} are applied, the inverter works in the first quadrant, exhibiting a suddenly voltage drop around $V_{DD}/2$ and a maximum gain of 20.5. When V_{DD} and V_{in} are negative, the inverter still operates the same behavior in the third quadrant with a maximum gain of 15.8. The gain value operated under V_{DD}= 30, 40, 50V and -30, -40, -50V are shown in Fig. 3(c). On the other hand, we compared the optimized electron mobility (7.51×10^{-2}cm^2/V s) of n-type nanofiber with the different mobilities of p-type nanofibers by controlling the diameters of P3HT nanofibers (at 0.1, 0.2, 0.3 mL/h core feed rate).[19,25] In Fig. S4 (ESI†), the P3HT fibers exhibited hole mobilities of 8.25×10^{-1} cm^2/V s, 2.63×10^{-3} cm^2/V s, and 9.72×10^{-5} cm^2/V s at diameters of 157, 282, and 466 nm, respectively. The unbalanced ambipolar mobilities resulted in larger noise margin from $V_{DD}/2$ and lower gain (12.2 and 6.1) than the balanced one (20.5), showing the lower conductivity of p-channel nanofiber changed the classical behavior of complementary inverters.[27]

In summary, we successfully fabricated the ambipolar FET and inverters based on paralleled nanofibers by using electrospinning method. The performance of the ambipolar nanofiber transistor

is much better than that of bilayer and heterojunction transistors, due to the extremely isolation of p-type and n-type polymers. These results indicate that electrospun method and ambipolar nanofiber transistors provides a facile way to construct organic electronics with not only elevated crystallinity and mobilities but also well-defined interfaces morphology to control the performance of organic electronics.

Acknowledgment

The financial supports from National Science Council of Taiwan and the Japan Science and Technology Agency (JST), PRESTO program (JY 220176) are highly appreciated.

Notes and references

1. N. J. Tremblay, B. J. Jung, P. Breysse and H. E. Katz, *Adv. Funct. Mater.*, 2011, **21**, 4314.
2. P. M. Beaujuge and J. M. J. Frechet, *J. Am. Chem. Soc.*, 2011, **133**, 20009.
3. C. L. Wang, H. L. Dong, W. P. Hu, Y. Q. Liu and D. B. Zhu, *Chem. Rev.*, 2012, **112**, 2208.
4. A. Dodabalapur, H. E. Katz, L. Torsi and R. C. Haddon, *Science*, 1995, **269**, 1560.
5. J. W. Shi, H. B. Wang, D. Song, H. Tian, Y. H. Geng and D. H. Yan, *Adv. Funct. Mater.*, 2007, **17**, 397.
6. S. D. Wang, K. Kanai, Y. Ouchi and K. Seki, *Org. Electron.*, 2006, **7**, 457.
7. F. Dinelli, R. Capelli, M. A. Loi, M. Murgia, M. Muccini, A. Facchetti and T. J. Marks, *Adv. Mater.*, 2006, **18**, 1416.
8. M. J. An, H. S. Seo, Y. Zhang, J. D. Oh and J. H. Choi, *Appl. Phys. Lett.*, 2010, **97**, 023506.
9. A. Babel, J. D. Wind and S. A. Jenekhe, *Adv. Funct. Mater.*, 2004, **14**, 891.
10. L. L. Chua, J. Zaumseil, J. F. Chang, E. C. W. Ou, P. K. H. Ho, H. Sirringhaus and R. H. Friend, *Nature*, 2005, **434**, 194.
11. M. Shkunov, R. Simms, M. Heeney, S. Tierney and I. McCulloch, *Adv. Mater.*, 2005, **17**, 2608.
12. K. Szendrei, D. Jarzab, Z. H. Chen, A. Facchetti and M. A. Loi, *J. Mater. Chem.*, 2010, **20**, 1317.
13. S. S. Cheng, P. Y. Huang, M. Ramesh, H. C. Chang, L. M. Chen, C. M. Yeh, C. L. Fung, M. C. Wu, C. C. Liu, C. Kim, H. C. Lin, M. C. Chen and C. W. Chu, *Adv. Funct. Mater.*, 2014, **24**, 2057.
14. H. B. Wang and D. H. Yan, *Npg Asia Mater*, 2010, **2**, 69.
15. S. J. Noever, S. Fischer and B. Nickel, *Adv. Mater.*, 2013, **25**, 2147.

16. S. W. Lee, H. J. Lee, J. H. Choi, W. G. Koh, J. M. Myoung, J. H. Hur, J. J. Park, J. H. Cho and U. Jeong, *Nano Lett.*, 2010, **10**, 347.
17. H. C. Chang, C. L. Liu and W. C. Chen, *Adv. Funct. Mater.*, 2013, **23**, 4960.
18. Y. W. Lin, C. J. Lin, Y. H. Chou, C. L. Liu, H. C. Chang and W. C. Chen, *J. Mater. Chem. C*, 2013, **1**, 5336.
19. J. Y. Chen, C. C. Kuo, C. S. Lai, W. C. Chen and H. L. Chen, *Macromolecules*, 2011, **44**, 2883.
20. E. V. Canesi, A. Luzio, B. Saglio, A. Bianco, M. Caironi and C. Bertarelli, *Acs Macro Lett*, 2012, **1**, 366.
21. X. G. Guo, F. S. Kim, M. J. Seger, S. A. Jenekhe and M. D. Watson, *Chem Mater*, 2012, **24**, 1434.
22. H. L. Chen, L. J. Li and T. L. Lin, *Macromolecules*, 1998, **31**, 2255.
23. S. R. Tseng, S. C. Lin, H. F. Meng, H. H. Liao, C. H. Yeh, H. C. Lai, S. F. Horng and C. S. Hsu, *Appl. Phys. Lett.*, 2006, **88**, 163501.
24. J. Zaumseil and H. Sirringhaus, *Chem. Rev.*, 2007, **107**, 1296.
25. C. J. Lin, J. C. Hsu, J. H. Tsai, C. C. Kuo, W. Y. Lee and W. C. Chen, *Macromol. Chem. Phys.*, 2011, **212**, 2452.
26. A. L. Briseno, S. C. B. Mannsfeld, C. Reese, J. M. Hancock, Y. Xiong, S. A. Jenekhe, Z. Bao and Y. Xia, *Nano Lett.*, 2007, **7**, 2847.
27. D. Khim, K. J. Baeg, B. K. Yu, S. J. Kang, M. Kang, Z. H. Chen, A. Facchetti, D. Y. Kim and Y. Y. Noh, *J. Mater. Chem. C*, 2013, **1**, 1500.

Table 1 Electrical properties of bilayer, binary blends, and two-channel nanofibers FET containing P3HT and P(NDI-T) with top gate/bottom contact device geometry, respectively.

	μ_h (cm^2/V s)	I_{on}/I_{off}	V_t (V)	μ_e (cm^2/V s)	I_{on}/I_{off}	V_t (V)
Bilayer	$(1.1\pm0.4)\times10^{-4}$	7	-16±5	$(5.1\pm2.9)\times10^{-5}$	3	16±3
Binary blends	$(5.3\pm0.1)\times10^{-5}$	2×10^{2}	18±5	$(1.7\pm0.2)\times10^{-5}$	6	29±1
Paralleled nanofibers	$(8.2\pm0.4)\times10^{-2}$	5×10^{4}	-9±1	$(7.5\pm0.3)\times10^{-2}$	3×10^{4}	19±2

* The μ_e of bilayer and binary blends transistors were measured under V_d= -30V, which is limited by that the value under V_d= 30V could not show electron transporting properties due to the sweeping range of V_g. The μ_e of two-channel nanofibers transistor were measured V_d= 30V. All the electrical characteristics were averaged on at least five devices from three different batches, and the mobilities were calculated in a range of 10 V.

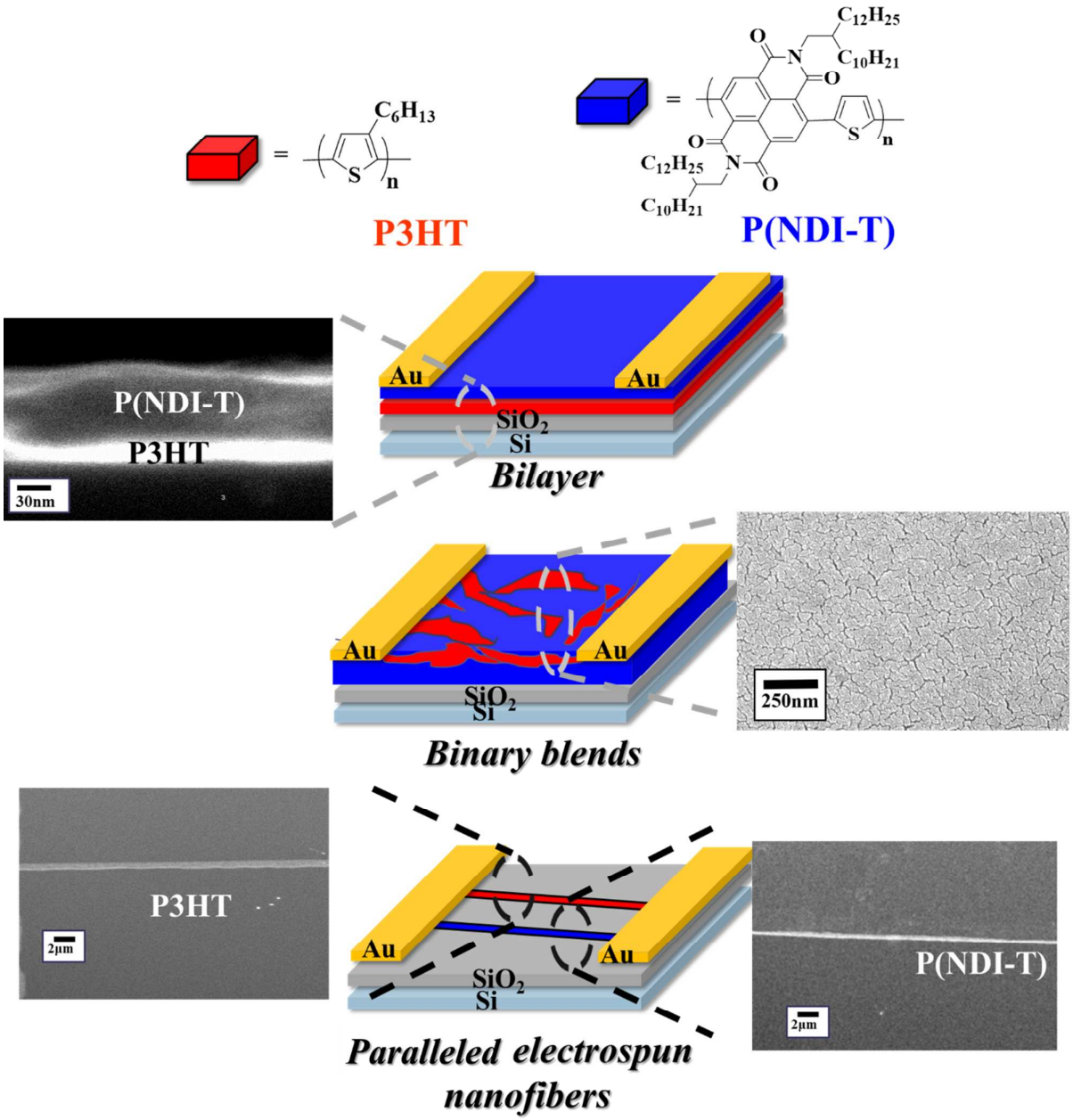

Fig. 1 The illustration of the bilayer, binary blends, and paralleled nanofibers transistor devices employed in this study with their surface images.

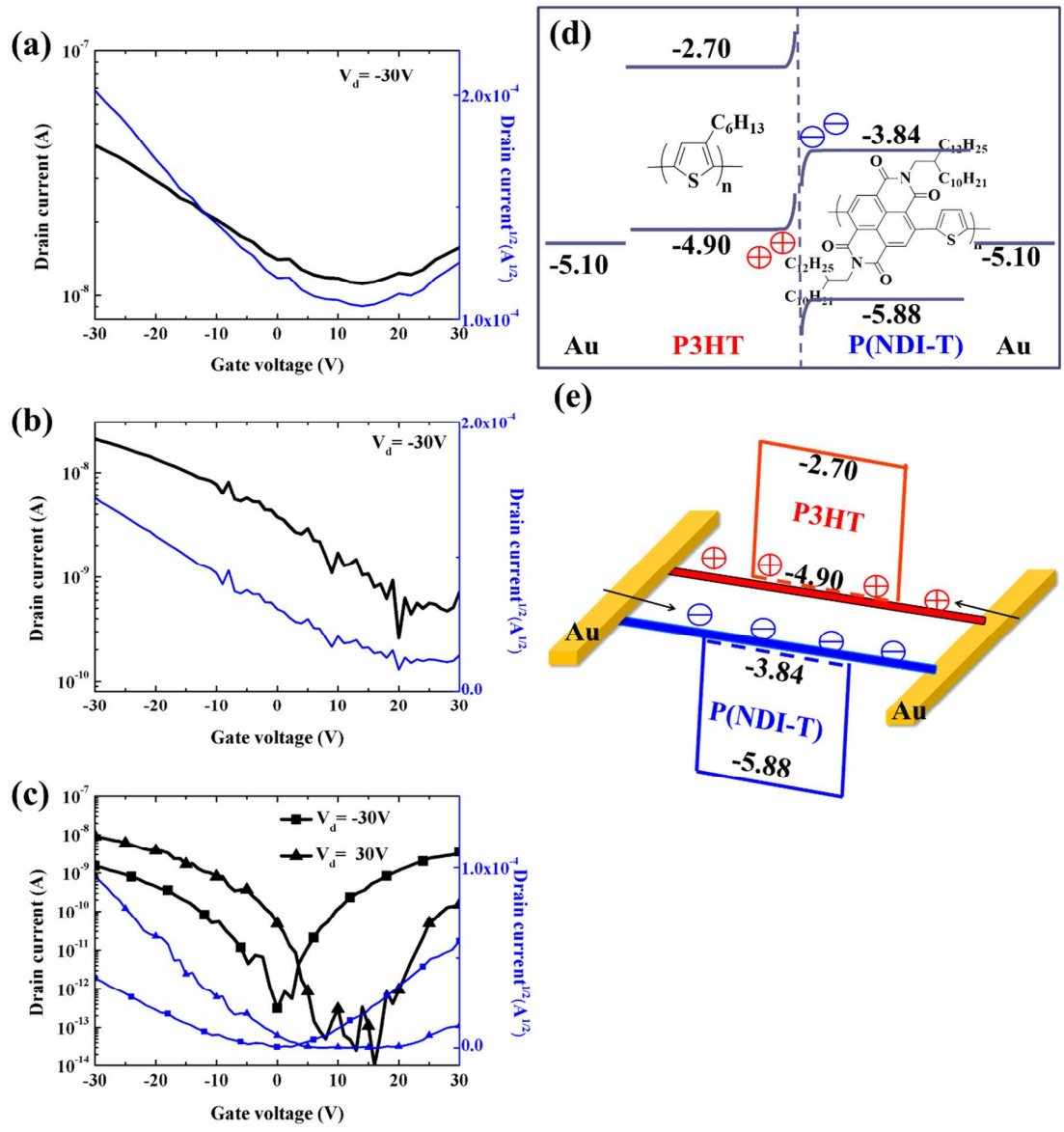

Fig. 2 Transfer characteristics of the ambipolar (a) bilayer, (b) binary blends, and (c) paralleled nanofibers FETs. Energy level diagrams for (d) P3HT and P(NDI-T) bilayer and binary blends, which directly contact with each other, and (e) P3HT and P(NDI-T) nanofibers.

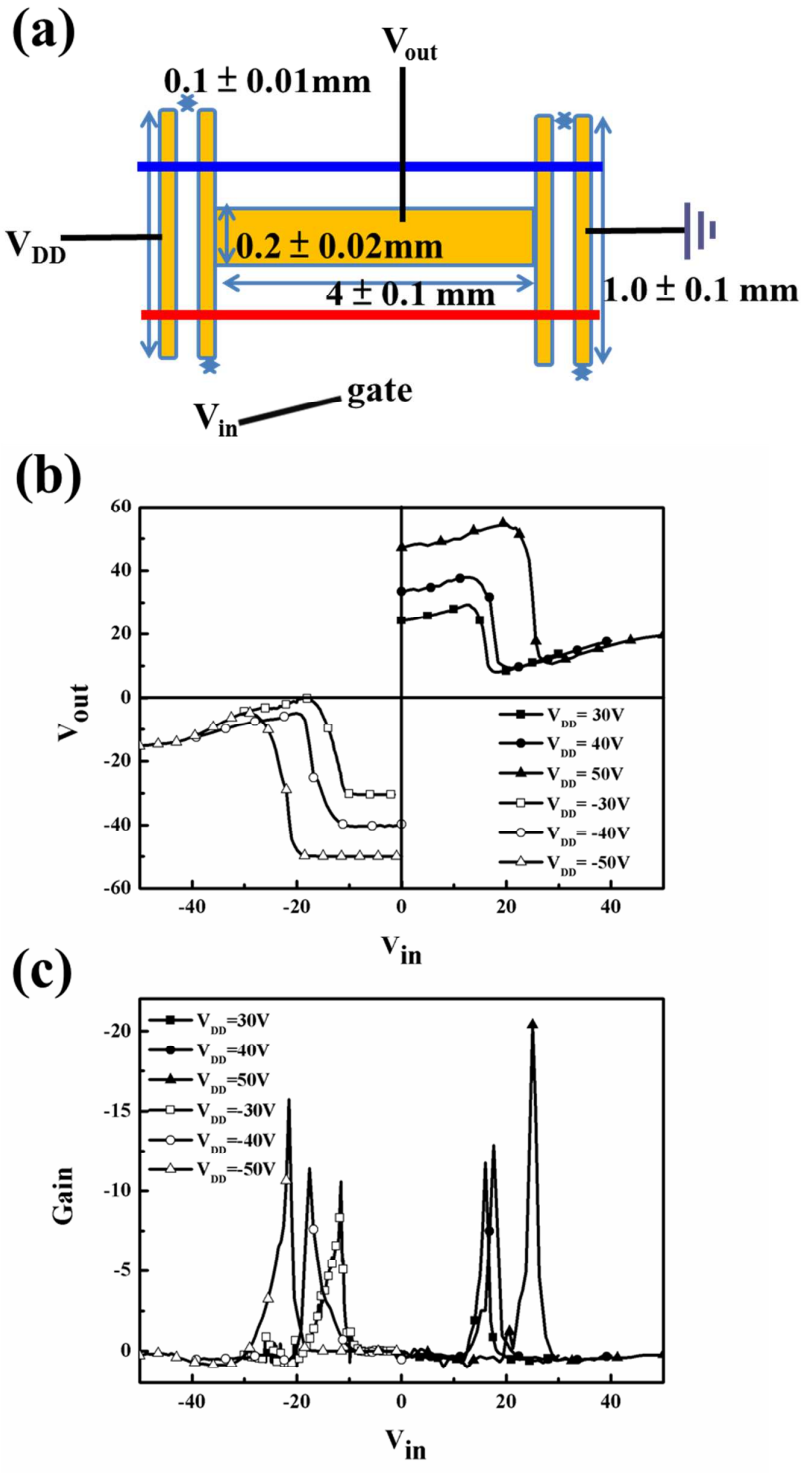

Fig. 3 (a) Paralleled electrospun nanofibers inverter architecture. (b) Voltage transfer characteristics at different supply voltage (V_{DD}) and (c) corresponding output voltage gains of the inverters

Table of contents entry

An ambipolar field-effect transistor using paralleled nanofibers showed high and well-balanced mobilities of holes (0.082 $cm^2V^{-1}s^{-1}$) and electrons (0.075 $cm^2V^{-1}s^{-1}$).